

² **Improved Neutrino-Induced-Muon Momentum**
³ **Determination by Multiple Coulomb Scattering in the**
⁴ **MicroBooNE LArTPC from Tuning the Highland**
⁵ **Formula**

⁶ **The MicroBooNE Collaboration**

⁷ ABSTRACT: We discuss a technique for measuring a charged particle's momentum by means of
⁸ multiple Coulomb scattering (MCS) in the MicroBooNE liquid argon time projection chamber
⁹ (LArTPC), which does not require the full particle ionization track to be contained inside of the
¹⁰ detector volume as other track momentum reconstruction methods do (range-based momentum
¹¹ reconstruction and calorimetric momentum reconstruction). We motivate use of this technique,
¹² prescribe a tuning of the underlying theory formula, quantify its performance on fully contained
¹³ beam-neutrino-induced muon tracks both in simulation and in data, and quantify its performance
¹⁴ on exiting muon tracks in simulation. We find agreement between data and simulation for con-
¹⁵ tained tracks, with a small bias in the momentum reconstruction and with resolutions that vary as a
¹⁶ function of track length, decreasing from about 10% for the shortest (one meter long) tracks to 5%
¹⁷ for longer (several meter) tracks. For exiting muons with at least one meter of track contained, we
¹⁸ find a similarly small bias, and a resolution which is better than 15% for muons with momentum
¹⁹ below 2 GeV/c though worse at higher momenta due to detector resolution effects.

20	Contents	
21	1 Introduction and Motivation	1
22	2 Multiple Coulomb Scattering (MCS)	3
23	2.1 Tuning the Highland Formula for Argon	3
24	3 MCS Implementation Using the Maximum Likelihood Method	6
25	3.1 Track Segmentation and Scattering Angle Computation	6
26	3.2 Maximum Likelihood Theory	7
27	3.3 Maximum Likelihood Implementation	7
28	4 Range-based Energy Validation from Simulation	7
29	5 MCS Performance on Beam Neutrino-Induced Muons in MicroBooNE Data	8
30	5.1 Input Sample	8
31	5.2 Event Selection	8
32	5.3 Highland Validation	10
33	5.4 MCS Momentum Validation	10
34	5.5 Impact of Highland Formula Tuning	11
35	6 MCS Performance on Exiting Muons in MicroBooNE Simulation	12
36	7 Conclusions	14

37 **1 Introduction and Motivation**

38 In this paper we summarize the theory of multiple Coulomb scattering (MCS) and describe how
39 the underlying Highland formula is retuned based on Monte Carlo simulation for use specifically in
40 liquid argon time projection chambers (LArTPCs). We present a maximum likelihood based algo-
41 rithm that is used to determine the momentum of particles in a LArTPC. The only way to determine
42 the momentum of a particle that exits a TPC is through MCS measurements. We demonstrate that
43 this technique works for a sample of fully contained muons from Booster Neutrino Neam (BNB)
44 ν_μ charged-current (CC) interactions, with bias and resolutions quantified. Additionally, quantifi-
45 cation of performance on exiting tracks is presented.

46
47 MicroBooNE (Micro Booster Neutrino Experiment) is an R&D experiment that uses a large
48 LArTPC to investigate the excess of low energy events observed by the MiniBooNE experiment
49 [1] and to study neutrino-argon cross-sections. MicroBooNE is part of the Short-Baseline Neutrino
50 (SBN) [2] physics program at the Fermi National Accelerator Laboratory (Fermilab) along with
51 two other LArTPCs: the Short Baseline Near Detector (SBND) and the Imaging Cosmic And Rare

52 Underground Signal (ICARUS) detector. MicroBooNE also performs important research and de-
53 velopment in terms of detector technology and event reconstruction techniques for future LArTPC
54 experiments including DUNE (Deep Underground Neutrino Experiment).

55

56 The MicroBooNE detector [3] consists of a rectangular time projection chamber (TPC) with
57 dimensions 2.6 m width \times 2.3 m height \times 10.4 m length located 470 m away from the Booster
58 Neutrino Beam (BNB) target. LArTPCs allow for precise three-dimensional reconstruction of par-
59 ticle interactions. The x - direction of the TPC corresponds to the drift coordinate, the y - direction
60 is the vertical direction, and the z - direction is the direction along the beam. The mass of active
61 liquid argon in the MicroBooNE TPC is 89 tons, with the total cryostat containing 170 tons of
62 liquid argon.

63

64 A set of 32 photomultiplier tubes (PMTs) and three planes of wires with 3 mm spacing at
65 angles of 0, and ± 60 degrees with respect to the vertical are located in the TPC for event recon-
66 struction. The cathode plane operating voltage is -70 kV. In a neutrino interaction, a neutrino from
67 the beam interacts with an argon nucleus and the charged outgoing secondary particles traverse the
68 medium, losing energy and leaving an ionization trail. The resulting ionization electrons drift to the
69 anode side of the TPC, containing the wire planes. The passage of these electrons past the first two
70 wire planes induces a signal in them, and their collection on the third plane also generates a signal.
71 These signals are used to create three distinct two-dimensional views (in terms of wire and time)
72 of the event. Combining these wire signals with timing information from the PMTs allows for full
73 three-dimensional reconstruction of the event. The fiducial volume used in this analysis is defined
74 as the full TPC volume reduced by 20 cm from both the cathode plane and the anode wire planes,
75 by 26.5 cm from both the top and bottom walls of the TPC, by 20 cm from the beam-entering wall
76 of the TPC, and by 36.8 cm from the beam-exiting wall of the TPC. This fiducial volume, corre-
77 sponding to a mass of 55 tons, was chosen to reduce the impact of electric field nonuniformities
78 near the edges of the TPC which have been characterized in parts of the TPC where the effect is
79 expected to be the largest, but not fully calibrated out in data [4].

80

81 The Booster Neutrino Beam (BNB) is predominantly composed of muon neutrinos (ν_μ) with
82 a peak neutrino energy of about 0.7 GeV, some of which undergo charge-current (ν_μ CC) interac-
83 tions in the TPC and produce muons. For muon tracks that are completely contained in the TPC,
84 it is straightforward to calculate their momentum with a measurement of the length of the parti-
85 cle's track, or with calorimetric measurements which come from wire signal size measurements.
86 Around half of the muons from BNB ν_μ CC interactions in MicroBooNE are not fully contained
87 in the TPC, and therefore using a length-based or calorimetry-based method to determine the mo-
88 ments for these uncontained tracks is not a possibility; the only way to determine their momenta is
89 through MCS.

90

91 **2 Multiple Coulomb Scattering (MCS)**

92 Multiple Coulomb scattering (MCS) occurs when a charged particle enters a medium and under-
93 goes electromagnetic scattering with atomic nuclei. This scattering perturbs the original trajectory
94 of the particle within the material (Figure 1). For a given initial momentum p , the angular deflection
95 scatters of a particle in either the x' direction or y' direction (as indicated in the aforementioned fig-
96 ure) form a Gaussian distribution centered at zero with an RMS width, σ_o^{HL} , given by the Highland
97 formula [5]:

$$\sigma_o^{HL} = \frac{S_2}{p\beta c} z \sqrt{\frac{\ell}{X_0}} \left[1 + \epsilon \times \ln\left(\frac{\ell}{X_0}\right) \right] \quad (2.1)$$

98 where β is the ratio of the particle's velocity to the speed of light assuming the particle is a muon,
99 ℓ is the distance traveled inside the material, z is the magnitude of the charge of the particle (unity,
100 for the case of muons), and X_0 is the radiation length of the target material (taken to be a constant
101 14 cm in liquid argon). S_2 and ϵ are constants defined to be 13.6 MeV and 0.0038, respectively.
102 In this study, a modified version of the Highland formula is used that includes a detector-inherent
103 angular resolution term, σ_o^{res}

$$\sigma_o = \sqrt{(\sigma_o^{HL})^2 + (\sigma_o^{res})^2} \quad (2.2)$$

104 For this analysis, the σ_o^{res} term is given a fixed value of 3 mrad which has been determined to be
105 an acceptable value based on simulation studies of higher momenta muons. At 4.5 GeV/c muon
106 momentum and $l \approx X_0$, Equation 2.1 predicts an RMS angular scatter of 3 mrad, comparable to the
107 detector resolution. The fully contained muons addressed in this analysis have momenta below 1.5
108 GeV/c, making detector resolution negligible.

109
110 With the Highland formula, the momentum of a track-like particle can be determined using
111 only the 3D reconstructed track it produces in the detector, without any calorimetric or track range
112 information. Within neutrino physics, past emulsion detectors like the DONUT [6] and OPERA
113 [7] experiments have used MCS to determine particle momenta. Additionally, the MACRO [8]
114 experiment at Gran Sasso Laboratory utilized this technique. While the original method for using
115 MCS to determine particle momentum in a LArTPC used a Kalman Filter and was described by
116 the ICARUS collaboration [9] (more recently the ICARUS collaboration describes another method
117 [10]), the maximum-likelihood based method discussed in this paper for use in the MicroBooNE
118 detector is described in detail in Section 3.

119 **2.1 Tuning the Highland Formula for Argon**

120 The Highland formula as written in Equation 2.1 originated from a 1991 publication by G. R. Lynch
121 and O. I. Dahl [11]. The constants in the equation (S_2 and ϵ) were determined using a global fit
122 over MCS simulated data using a modified GEANT simulation package of 14 different elements
123 and 7 thickness ranges. All of the simulated particles were relativistic, with $\beta = 1$. The materials
124 in which they studied scattering ranged from hydrogen (with Z=1) to uranium (with Z=92). Given
125 that the constants in the formula were determined from a single fit to a wide range of Z with a
126 wide range of material thicknesses, there is reason to believe that these constants should differ for

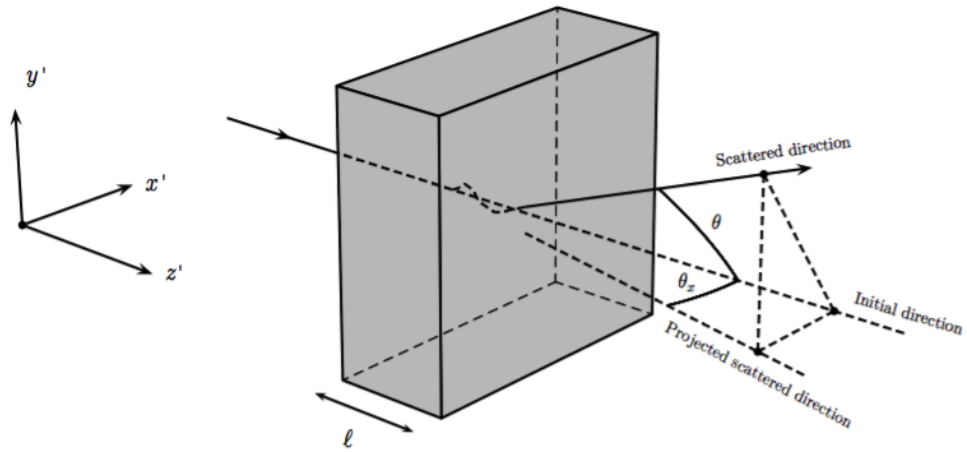


Figure 1. The particle's trajectory is deflected as it traverses through the material.

scattering specifically in liquid argon with $l \approx X_0$. There is also reason to believe that these constants might be momentum-dependent for particles with $\beta < 1$, which is the case for some of the contained muons in this analysis.

130

131 In order to re-tune these constants to liquid argon, a large sample of muons were simulated
 132 with GEANT4 [12] in the MicroBooNE TPC and their true angular scatters were used in a fit,
 133 with $l = X_0$. The reason for using $l = X_0$ is that the Highland formula simplifies to remove its
 134 dependence on the ϵ constant term:

$$\sigma_o^{HL} = \frac{S_2}{p\beta c} \quad (2.3)$$

135 The S_2 constant in Equation 2.3 was fit for as a function of true muon momentum at each
 136 scatter, in order to explore the β dependence of this constant. The fitted constant value as a function
 137 of true momentum is shown in Figure 2.

138 It can be seen that the fitted value of S_2 is always less than the nominal 13.6 for momentum
 139 greater than 0.25 GeV/c and asymptotically approaches a constant at higher momentum (where
 140 $\beta = 1$) of about 11.0. The value increases in the momentum region where $\beta < 1$. Shown in red
 141 is a fit to these data points with functional form $\frac{a}{p^2} + c$, with best fit values for floating constants a
 142 and c being 0.105 and 11.004 respectively. This functional form was chosen because it fit the data
 143 well, and asymptotically approaches a constant value when β approaches 1. This function, used as
 144 a replacement for the S_2 constant in the Highland formula, will henceforth be referred to as $\kappa(p)$:

$$\kappa(p) = \frac{0.105}{p^2} + 11.004 \quad (2.4)$$

145 To visualize the Highland formula for $l = X_0$ both before and after the $\kappa(p)$ replacement,
 146 see Figure 3. It is recommended that future LArTPC experiments use this parameterization of the
 147 Highland formula, or at the very least conduct their own studies to tune the Highland formula for

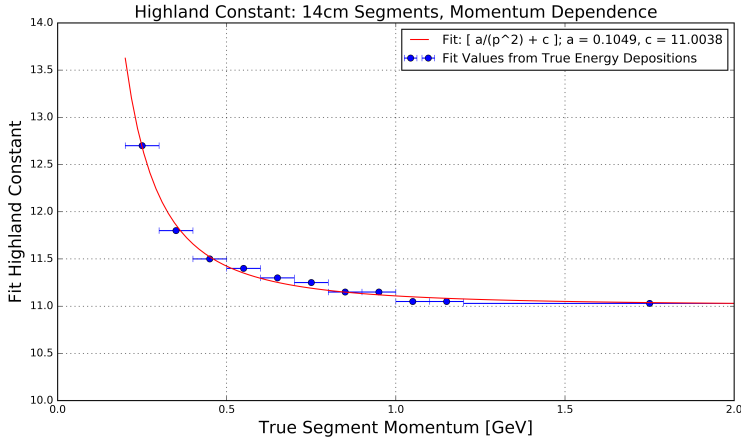


Figure 2. Fitted Highland constant S_2 as a function of true segment momentum for $\ell = X_0$ simulated muons in the MicroBooNE LArTPC. Blue x- error bars indicate the true momentum bin width with data points drawn at the center of each bin. Shown in red is a fit to these data points with functional form $\frac{a}{p^2} + c$, with best fit values for constants a and c shown in the legend.

148 scattering specifically in argon. This formulation can also be checked in LAr-based test-beam experiments like LArIAT [13].
 149
 150

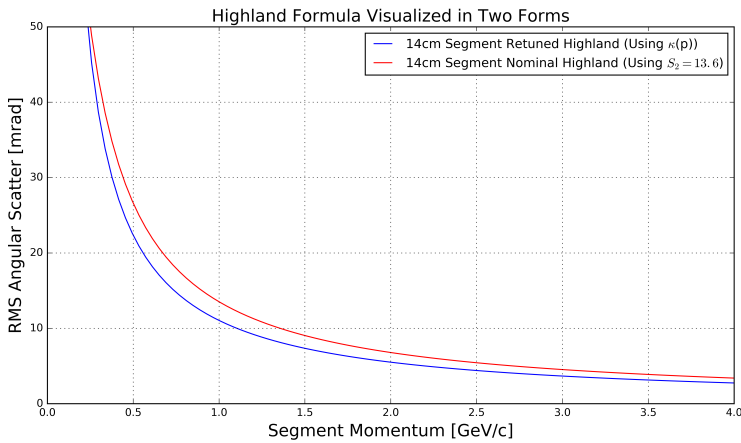


Figure 3. The Highland scattering RMS σ_o for 14 cm segment lengths and 0 detector-inherent angular resolution as a function of true momentum before and after tuning. In red is shown Equation 2.3 (the nominal Highland formula using $S_2 = 13.6$) and in blue is the retuned Highland formula (replacing S_2 with $\kappa(p)$).

151 With $\ell = X_0$, the form of the Highland equation used in this analysis is therefore:

$$\sigma_o^{RMS} = \sqrt{(\sigma_o)^2 + (\sigma_o^{res})^2} = \sqrt{\left(\frac{\kappa(p)}{p\beta c}\right)^2 + (\sigma_o^{res})^2} \quad (2.5)$$

152 **3 MCS Implementation Using the Maximum Likelihood Method**

153 This section describes exactly how the phenomenon of multiple Coulomb scattering is leveraged
154 to determine the momentum of a muon track reconstructed in a LArTPC. In general, the approach
155 is as follows:

- 156 1. The three-dimensional track is divided into segments of configurable length.
- 157 2. The scattering angles between consecutive segments are measured.
- 158 3. Those angles combined with the modified, tuned Highland formula (Equation 2.5) are used
159 to build a likelihood that the particle has a specific momentum, taking into account energy
160 loss in upstream segments of the track.
- 161 4. The momentum corresponding to the maximum of the likelihood is chosen to be the MCS
162 computed momentum.

163 Each of these steps is discussed in detail in the following subsections.

164

165 **3.1 Track Segmentation and Scattering Angle Computation**

166 Track segmentation refers to the subdivision of three-dimensional reconstructed trajectory points
167 of a reconstructed track into portions of definite length. In this analysis, the tracks are automati-
168 cally reconstructed by the “pandoraNuPMA” projection matching algorithm which constructs the
169 three-dimensional trajectory points by combining two-dimensional hits reconstructed from signals
170 on the different wire planes along with timing information from the photomultiplier tubes [14].
171 The segmentation routine begins at the start of the track, and iterates through the trajectory points
172 in order, defining segment start and stop points based on the straight-line distance between them.
173 There is no overlap between segments. Given the subset of the three-dimensional trajectory points
174 that corresponds to one segment of the track, a three-dimensional linear fit is applied to the data
175 points, weighting all trajectory points equally in the fit. In this analysis, a segment length of 14 cm
176 is used, which is a tunable parameter that has been chosen as described in the derivation of $\kappa(p)$
177 (Equation 2.4).

178

179 With the segments defined, the scattering angles between the linear fits from adjacent segments
180 are computed. A coordinate transformation is performed such that the z' direction is oriented along
181 the direction of the linear fit to the first of the segment pair. The x' and y' coordinates are then
182 defined such that all of x' , y' , and z' are mutually orthogonal and right-handed, as shown in Figure
183 1. The scattering angles both with respect to the x' direction and the y' direction are then computed
184 to be used by the MCS algorithm. Note that only the scattering angle with respect to the x' direction
185 is drawn in Figure 1.

186 **3.2 Maximum Likelihood Theory**

187 The normal probability distribution for a scattering angle in either the x' or y' direction, $\Delta\theta$ with
188 an expected gaussian error σ_o and mean of zero is given by:

$$f_X(\Delta\theta) = (2\pi\sigma_o^2)^{-\frac{1}{2}} \exp\left(-\frac{1}{2}\left(\frac{\Delta\theta}{\sigma_o}\right)^2\right) \quad (3.1)$$

189 Here, σ_o is the RMS angular deflection computed by the modified, tuned Highland formula
190 (Equation 2.5), which is a function of both the momentum and the length of that segment. Since
191 energy is lost between segments along the track, σ_o increases for each angular measurement along
192 the track so we replace σ_o with $\sigma_{o,j}$, where j is an index representative of the segment.

193 To get the likelihood, one takes the product of $f_X(\Delta\theta_j)$ over all n of the $\Delta\theta_j$ segment-to-
194 segment scatters along the track. With some manipulation, this product becomes
195

$$L(\sigma_{o,1}, \dots, \sigma_{o,n}; \Delta\theta_1, \dots, \Delta\theta_n) = (2\pi)^{-\frac{n}{2}} \times \prod_{j=1}^n (\sigma_{o,j})^{-1} \times \exp\left(-\frac{1}{2} \sum_{j=1}^n \left(\frac{\Delta\theta_j}{\sigma_{o,j}}\right)^2\right) \quad (3.2)$$

196 In practice, rather than maximizing the likelihood it is more computationally convenient to
197 instead minimize the negative log likelihood. Inverting the sign and taking the natural logarithm of
198 the likelihood L gives an expression that is related to a χ^2

$$-l(\mu_o; \sigma_{o,1}, \dots, \sigma_{o,n}; \Delta\theta_1, \dots, \Delta\theta_n) = -\ln(L) = \frac{n}{2} \ln(2\pi) + \sum_{j=1}^n \ln(\sigma_{o,j}) + \frac{1}{2} \sum_{j=1}^n \left(\frac{\Delta\theta_j}{\sigma_{o,j}}\right)^2 \quad (3.3)$$

199 **3.3 Maximum Likelihood Implementation**

200 Given a set of angular deflections in the x' and y' directions for each segment as described in
201 Section 3.1 a raster scan over the postulated initial energy, E_t , in steps of 1 MeV up to 7.5 GeV is
202 computed and the step with the smallest negative log likelihood (Equation 3.3) is chosen as the final
203 MCS energy. Note that Equation 3.3 includes a $\sigma_{o,j}$ term which changes for consecutive segments
204 because their energy is decreasing. The energy of the j th segment is related to E_t by

$$E_j = E_t - E_j^{\text{upstream}} \quad (3.4)$$

205 where E_j^{upstream} is the energy loss upstream of this segment, computed by integrating the muon
206 stopping power curve given by the Bethe-Bloch equation described by the Particle Data Group
207 (PDG) [16] along the length of track upstream of this segment. Note that Equation 3.4 introduces a
208 minimum allowable track energy determined by the length of the track, as E_j must remain positive.
209 This value of segment energy is converted to a momentum, p , with the usual energy-momentum
210 relation assuming the muon mass, and is then used to predict the RMS angular scatter for that
211 segment (σ_o) by way of Equation 2.5.

212 **4 Range-based Energy Validation from Simulation**

213 In order to quantify the performance of the MCS energy estimation method on fully contained
214 muons in data, an additional handle on energy is needed. Here, range-based energy, E_{range} is used

215 since when dealing with data the true energy, E_{true} will not be known. The stopping power of
 216 muons in liquid argon is well described by the continuous-slowing-down-approximation (CSDA)
 217 by the particle data group (PDG) with agreement to data at the sub-percent level [15] [17] [18].
 218 By using a linear interpolation between points in the cited PDG stopping power table, the length
 219 of a track can be used to reconstruct the muon’s total energy with good accuracy. A simulated
 220 sample of fully contained BNB neutrino-induced muons longer than one meter is used to quantify
 221 the bias and resolution for the range-based energy estimation technique. The range is defined
 222 as the straight-line distance between the true starting point and true stopping point of a muon,
 223 even though the trajectories are not in fact perfectly straight lines. The bias and resolution are
 224 computed in bins of true total energy of the muons by fitting a gaussian to a distribution of the
 225 fractional energy difference ($\frac{E_{\text{Range}} - E_{\text{True}}}{E_{\text{True}}}$) in each bin. The mean of each gaussian indicates
 226 the bias for that true energy bin, and the width indicates the resolution. Figure 4 shows the bias
 227 and resolution for the range-based energy reconstruction method. It can be seen that the bias is
 228 negligible and the resolution for this method of energy reconstruction increases slightly with true
 229 muon energy but remains on the order of 2-4%. Based on this figure, it is clear that range-based
 230 energy (and therefore range-based momentum) is a good handle on the true energy (momentum)
 231 of a reconstructed contained muon track in data, assuming that the track is well reconstructed in
 232 terms of length.

233 5 MCS Performance on Beam Neutrino-Induced Muons in MicroBooNE Data

234 5.1 Input Sample

235 The input sample to this portion of the analysis is $\sim 5 \times 10^{19}$ protons-on-target worth of trig-
 236 gered BNB neutrino interactions in MicroBooNE data, which is a small subset (less than 10%)
 237 of the nominal amount of beam scheduled to be delivered to the detector. These events are run
 238 through a fully automated reconstruction chain which produces reconstructed objects including
 239 three-dimensional neutrino interaction points (vertices), three-dimensional tracks (as described in
 240 Section 3.1) for each outgoing secondary particle from the interaction, and PMT-reconstructed op-
 241 tical flashes from the interaction scintillation light. The fiducial volume used in this analysis is
 242 defined in Section 1.

243 5.2 Event Selection

244 The following selection cuts are placed on the aforementioned reconstructed objects to select ν_μ
 245 charged-current interactions in which a candidate muon track exiting the interaction vertex is fully
 246 contained within the fiducial volume:

- 247 1. The event must have at least one bright optical flash in coincidence with the expected BNB
 248 neutrino arrival time.
- 249 2. Two or more reconstructed tracks must originate from the same reconstructed vertex within
 250 the fiducial volume.
- 251 3. The span in $z-$ of the candidate muon track must be within 70 cm of the $z-$ position of the
 252 optical flash as determined by the pulse height and timing of signals in the 32 PMTs.

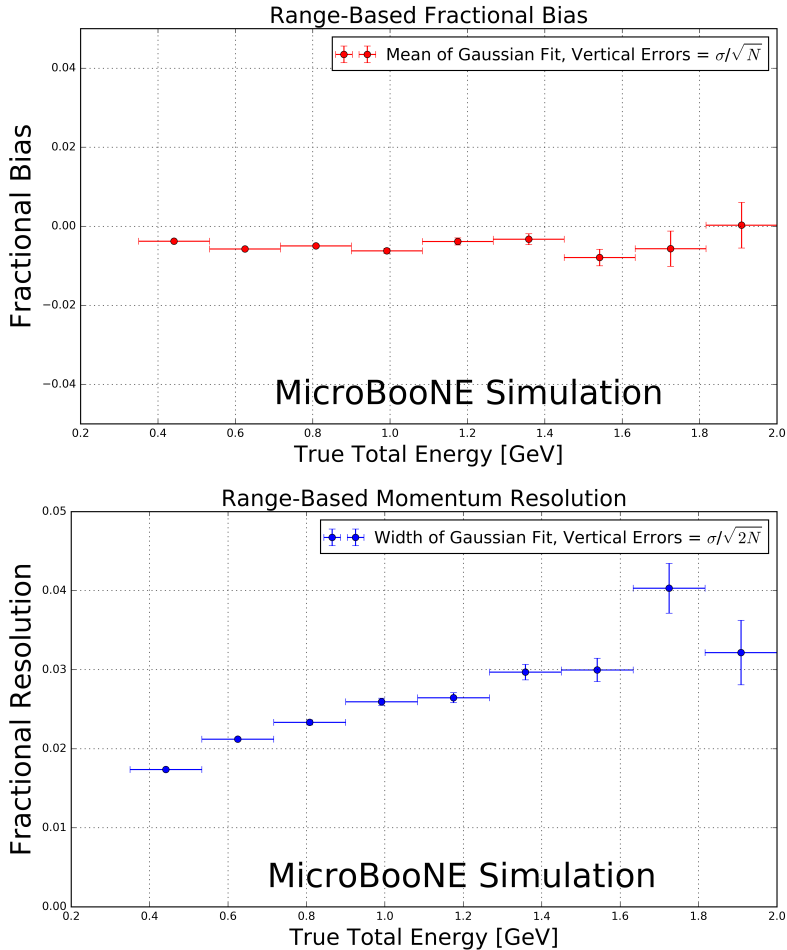


Figure 4. Range-based energy fractional bias (top) and resolution (bottom) from a sample of simulated fully contained BNB neutrino-induced muons using true starting and stopping positions of the track. The bias is less than 1% and the resolution is below $\approx 4\%$.

- 253 4. For events with exactly two tracks originating from the vertex, additional calorimetric-based
- 254 cuts are applied to mitigate backgrounds from cosmics in time with the passage of the beam
- 255 which produce a Michel electron reconstructed as a track.

- 256 5. The longest track originating from the vertex is assumed to be a muon, and it must be fully
- 257 contained within the fiducial volume.

- 258 6. The longest track must be at least one meter long, in order to have enough sampling points
- 259 in the MCS likelihood to obtain a reasonable estimate of its momentum.

260 These cuts were chosen to select a sample of tracks with high purity. In this sample of Micro-
 261 BooNE data, 598 events (tracks) remain after all event selection cuts. The relatively low statistics
 262 in this sample is due to the limited input sample, described in Section 5.1. Each of these events
 263 (tracks) were scanned by hand with a 2D interactive event display showing the raw wire signals of
 264 the interaction from each wire plane, with the 2D projection of the reconstructed muon track and

vertex overlaid. The scanning was done to ensure the track was well reconstructed with start point close to the reconstructed vertex and end point close to the end of the visible wire-signal track in all three planes. Additionally the scanning was to remove obvious mis-identification (MID) topologies such as cosmic rays inducing Michel electrons at the reconstructed neutrino vertex which were not successfully removed by the automated event selection cuts. After rejecting events (tracks) based on hand scanning, 396 tracks remain for analysis.

5.3 Highland Validation

The Highland formula indicates that histograms of the track segment-by-segment angular deviations in both the x' and y' directions divided by the width predicted from the Highland equation σ_o^{HL} (Equation 2.5) should be gaussian with a width of unity. In order to calculate the momentum p in the Highland equation, p for each segment is computed with Equation 3.4 where E_t comes from the converged MCS computed momentum of the track. For each consecutive pair of segments in this sample of 396 tracks, the angular scatter in milliradians divided by the Highland expected RMS in milliradians is an entry in the area-normalized histogram shown in Figure 5. From this figure we can see that the distribution has an RMS of unity, thus validating the MCS technique used in this analysis.

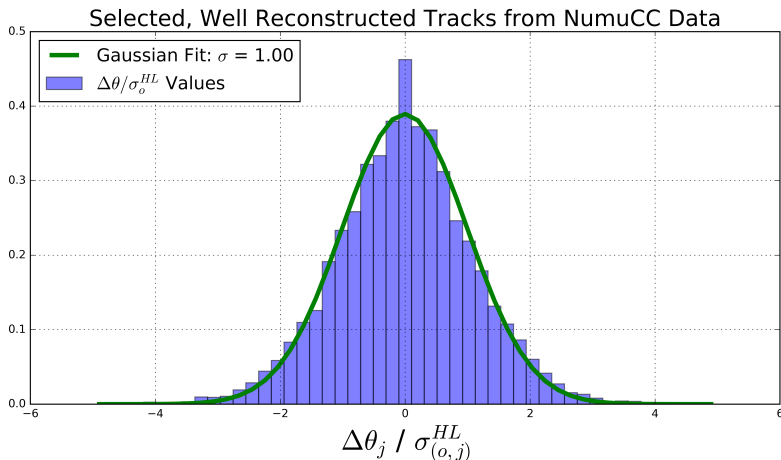


Figure 5. Segment-to-segment measured angular scatters in both the x' and y' directions divided by the Highland formula (Equation 2.1) predicted width σ_o^{HL} for the automatically selected beam neutrino-induced fully contained muon sample in MicroBooNE data after hand scanning to remove poorly reconstructed tracks and obvious mis-identification (MID) topologies. That the fitted Gaussian distribution has a width of unity indicates that the basis of the MCS technique is validated.

5.4 MCS Momentum Validation

The MCS momentum versus range-based momentum for this sample of 396 tracks can be seen in Figure 6. The fractional bias and resolution as a function of range-based momentum for this sample is shown in Figure 7. In order to compute this bias and resolution, distributions of fractional inverse momentum difference ($\frac{p_{MCS}^{-1} - p_{Range}^{-1}}{p_{Range}^{-1}}$) in bins of range-based momentum p_{Range}

286 are fit to gaussians and the mean of the fit determines the bias while the width of the fit determines
 287 the resolution for that bin. Inverse momentum is used here because the binned distributions are
 288 more gaussian (since the Highland formula measures inverse momentum in terms of track angles
 289 that have reasonably Gaussian errors). Note that simply using the mean and RMS of the binned
 290 distributions yields similar results. Also shown in this figure are the bias and resolutions for an anal-
 291 ogous simulated sample consisting of full BNB simulation with CORSIKA-generated [19] cosmic
 292 overlays passed through an identical reconstruction and event selection chain. Rather than hand
 293 scanning this sample, true simulation information was used by requiring the longest reconstructed
 294 track matched well in terms of true starting and stopping point of the ν_μ CC muon. This removes
 295 any mis identifications or interference from the simulated cosmics.

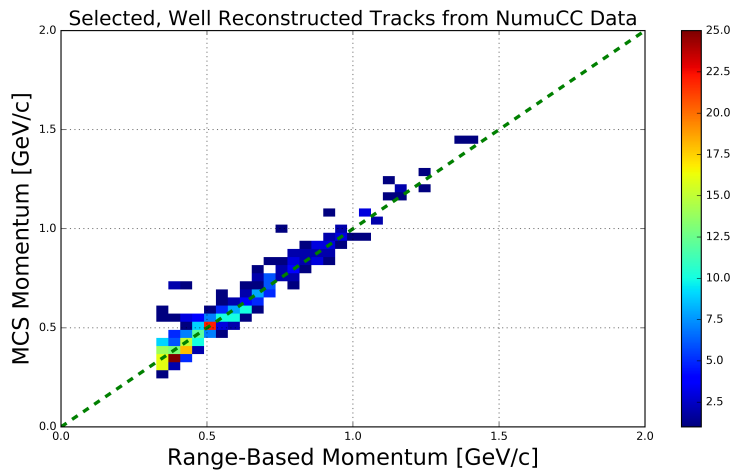


Figure 6. *MCS computed momentum versus range momentum for the automatically selected beam neutrino-induced fully contained muon sample in MicroBooNE data after hand scanning to remove poorly reconstructed tracks and obvious mis-identification (MID) topologies. The color (z) scale indicates number of tracks.*

296 Figure 7 indicates a bias in the MCS momentum calculation on the order of a few percent, with
 297 a resolution that decreases from about 10% for contained reconstructed tracks in data and simula-
 298 tion with range momentum around 0.45 GeV/c (which corresponds to a length of about 1.5 meters)
 299 to below 5% for contained reconstructed tracks in data and simulation with range momentum about
 300 1.15 GeV/c (which corresponds to a length of about 4.6 meters). Resolution improving with length
 301 of track is intuitive; the longer the track, the more angular scattering measurements can be made
 302 to improve the likelihood. In general the bias and resolutions agree between data and simulation
 303 within uncertainty.
 304

305 5.5 Impact of Highland Formula Tuning

306 In order to examine the impact of the Highland formula tuning described in Section 2.1, the frac-
 307 tional bias and resolution on the simulated sample of contained muons described in Section 5.4
 308 both with the nominal Highland formula (Equation 2.2) and with the retuned Highland formula
 309 (Equation 2.5) are shown in Figure 8. Tuning the Highland formula improves the magnitude of

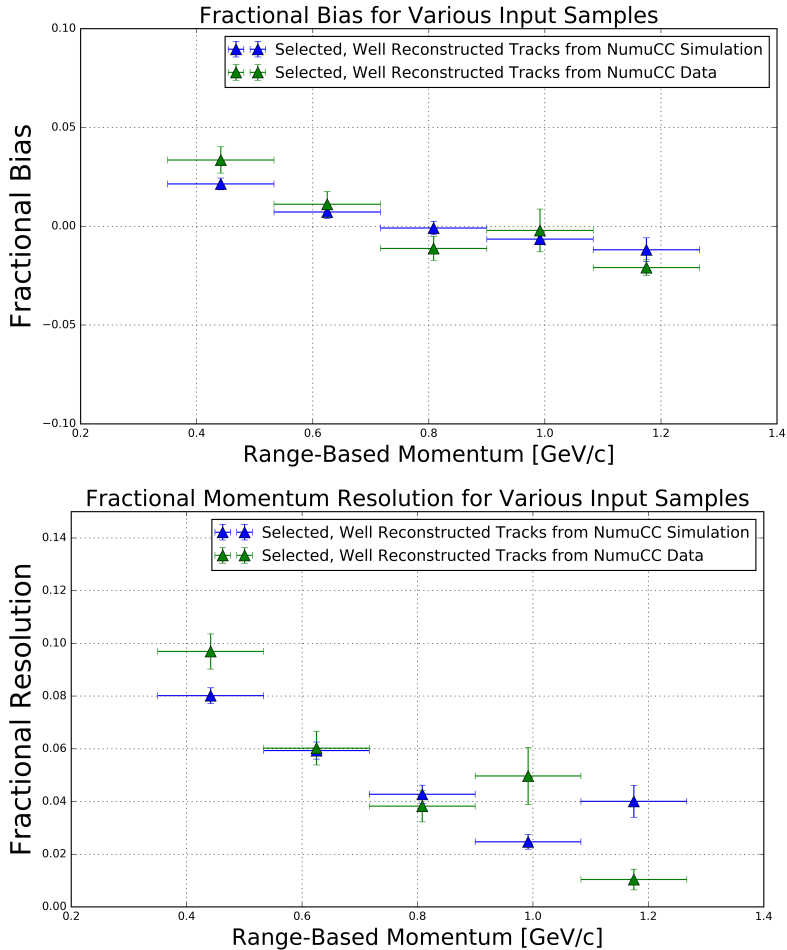


Figure 7. Inverse momentum difference (as defined in the text) fractional bias (top) and resolution (bottom) for automatically selected contained ν_μ CC-induced muons from full simulated BNB events with cosmic overlay where the track matches with the true muon track (blue), and automatically selected (see text) contained ν_μ CC-induced muons from MicroBooNE data (green).

the fractional bias to below 2%, and improves the fractional resolution by 2-3%, with the most improvement in the lowest momentum bins.

6 MCS Performance on Exiting Muons in MicroBooNE Simulation

This section quantifies the MCS algorithm performance on a sample of exiting muon tracks in simulated BNB ν_μ CC interactions within the MicroBooNE detector. The tracks are automatically reconstructed by the same “pandoraNuPMA” algorithm described in Section 3.1, and all tracks have at least one meter contained within the TPC. This simulation does not include space charge effects which are non-negligible near the TPC walls. The MCS momentum versus true momentum for this sample of 28,000 exiting muon tracks can be seen in Figure 9.

319

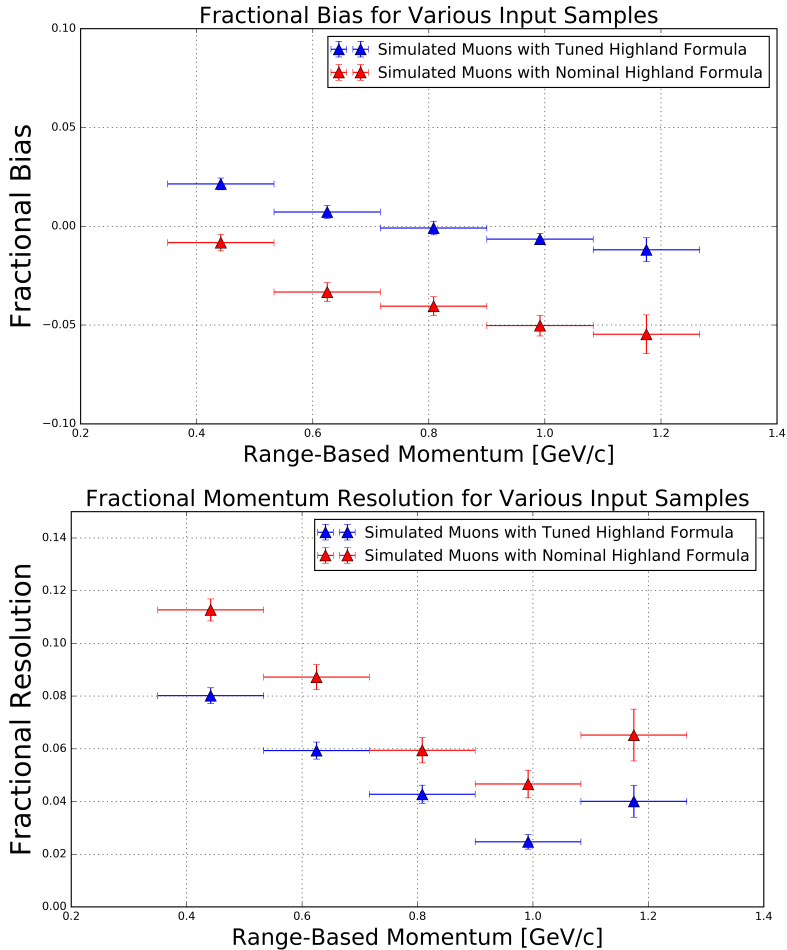


Figure 8. Inverse momentum difference (as defined in the text) fractional bias (top) and resolution (bottom) for automatically selected contained ν_μ CC-induced muons from full simulated BNB events with cosmic overlay where the track matches with the true muon track both using the nominal Highland formula (Equation 2.2) (red) and the retuned Highland formula (Equation 2.5) (blue).

320 The distribution of $(\frac{p_{MCS}^{-1} - p_{true}^{-1}}{p_{true}^{-1}})$ is shown for four representative bins of true momentum in
 321 Figure 10, along with the Gaussian fit to each. Low momentum tails in which the MCS momentum
 322 is an underestimation of the true momentum can be seen outside of the central gaussian fit. These
 323 tails can be attributed to reconstruction effects.
 324

325 The algorithm fractional bias and resolution as a function of true momentum are shown in Fig-
 326 ure 11. It can be seen that the bias is below 4% for all momenta, and the resolution is roughly 14%
 327 in the relevant momentum region for BNB ν_μ CC muons (below 2 GeV/c). The resolution worsens
 328 for muon momenta above this region because the angular scatters begin to be comparable with the
 329 detector resolution term of 3 mrad. Note that the resolution improves for longer lengths of track
 330 contained, with 10% resolution for muons below 2 GeV/c with more than 3.5 meters contained.
 331

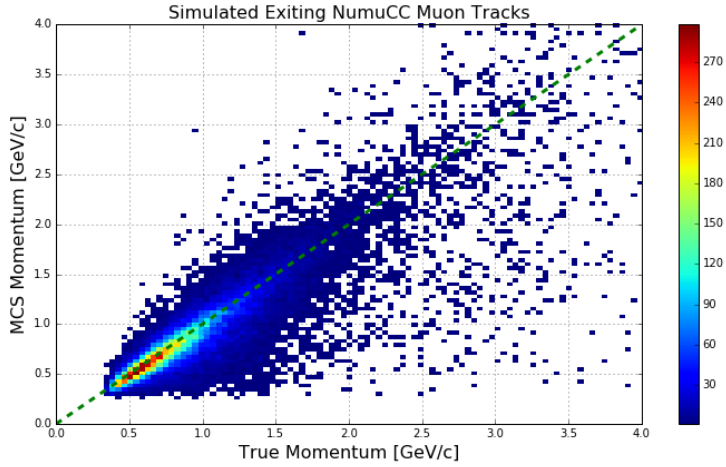


Figure 9. MCS computed momentum versus true momentum for the sample of simulated exiting BNB ν_μ CC muons in MicroBooNE with at least one meter of track contained within the TPC.

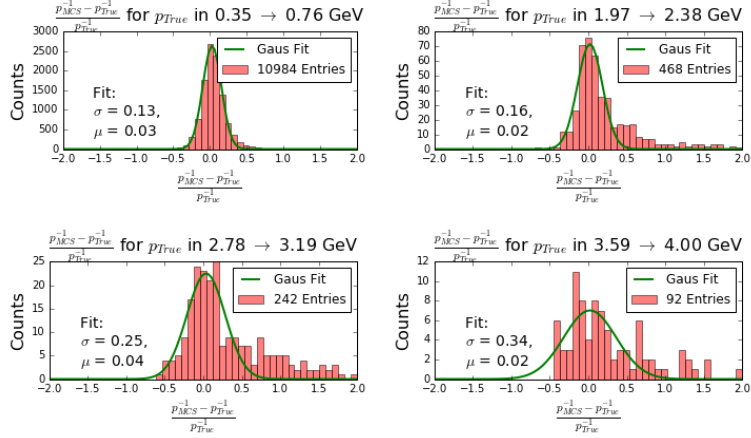


Figure 10. Fractional momentum difference for a few representative bins of true momentum.

332 7 Conclusions

333 We have described a multiple Coulomb scattering maximum likelihood method for estimating the
 334 momentum of a three dimensional reconstructed track in a LArTPC and have provided motivation
 335 for development of such a technique. Using MC, we have shown that the standard Highland formula
 336 should be re-tuned specifically for scattering in liquid argon. After benchmarking range-based
 337 momentum determination techniques with MicroBooNE MC, we have demonstrated the accuracy
 338 and precision of the MCS-based momentum reconstruction in MicroBooNE data by comparing its
 339 performance to the range-based method. For 398 fully-contained BNB ν_μ CC-induced muons, the
 340 MCS method exhibits a fractional bias below 3% and a momentum resolution below 10%, agreeing
 341 with simulation predictions. Using MC simulation of uncontained muon tracks in MicroBooNE
 342 with at least one meter contained, the MCS-based reconstruction is shown to produce a fractional
 343 bias below 4% and a momentum resolution of better than 15% for muons in the relevant BNB

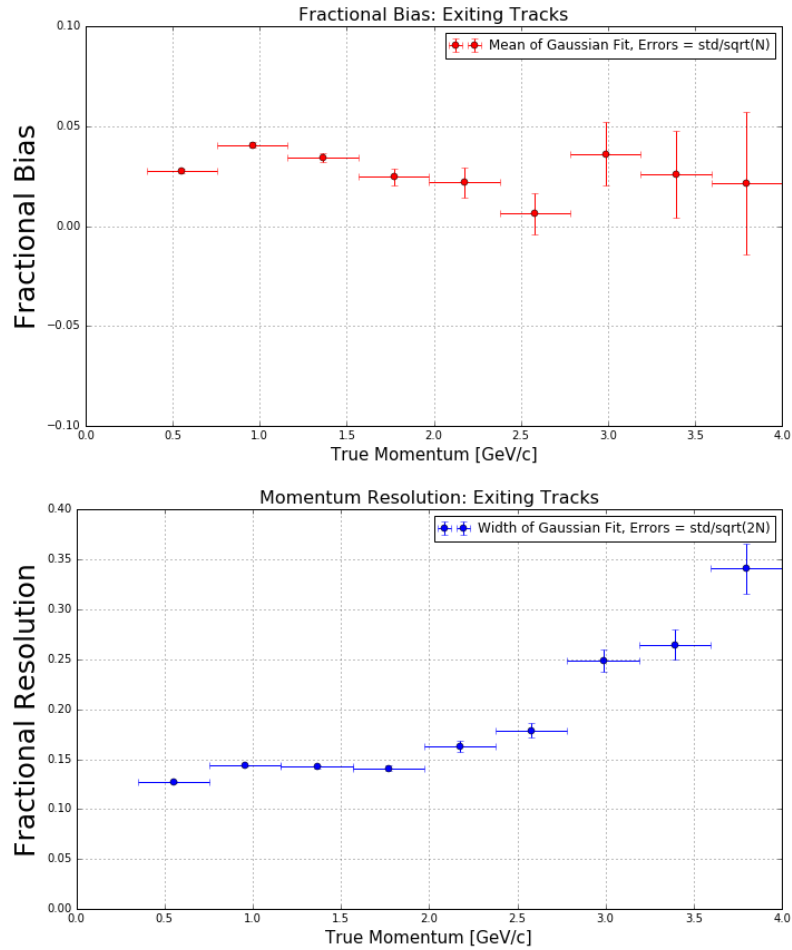


Figure 11. MCS momentum fractional bias (top) and resolution (bottom) as a function of true momentum from a sample of exiting reconstructed muon tracks.

344 energy region of below 2 GeV.

345 **References**

- 346 [1] A. A. Aguilar-Arevalo *et al.* [MiniBooNE Collaboration], Improved Search for $\bar{\nu}_\mu \rightarrow \bar{\nu}_e$ Oscillations
347 in the MiniBooNE Experiment, Phys. Rev. Lett. **110**, 161801 (2013).
348 doi:10.1103/PhysRevLett.110.161801 [arXiv:1207.4809 [hep-ex], arXiv:1303.2588 [hep-ex]].
- 349 [2] C. Adams *et al.* [LArTPC Collaboration], arXiv:1309.7987 [physics.ins-det].
- 350 [3] R. Acciarri *et al.* [MicroBooNE Collaboration], “Design and Construction of the MicroBooNE
351 Detector,” arXiv:1612.05824 [physics.ins-det].
- 352 [4] R. Acciarri *et al.* [MicroBooNE Collaboration], “Study of Space Charge Effects in MicroBooNE”
353 www-microboone.fnal.gov/publications/publicnotes/MICROBOONE-NOTE-1018-PUB.pdf.
- 354 [5] V. L. Highland, Some Practical Remarks on Multiple Scattering, Nucl. Instrum. Methods **129** (1975)
355 104-120.
- 356 [6] K. Kodama *et al.* [DONUT Collaboration], Phys. Lett. B **504**, 218 (2001)
357 doi:10.1016/S0370-2693(01)00307-0 [hep-ex/0012035].
- 358 [7] N. Agafonova *et al.* [OPERA Collaboration], New J. Phys. **14**, 013026 (2012)
359 doi:10.1088/1367-2630/14/1/013026 [arXiv:1106.6211 [physics.ins-det]].
- 360 [8] G. Giacomelli [MACRO Collaboration], Braz. J. Phys. **33**, 211 (2003)
361 doi:10.1590/S0103-97332003000200008 [hep-ex/0210006].
- 362 [9] A. Ankowski *et al.* [ICARUS Collaboration], “Measurement of through-going particle momentum by
363 means of multiple scattering with the ICARUS T600 TPC,” Eur. Phys. J. C **48**, 667 (2006)
364 doi:10.1140/epjc/s10052-006-0051-3 [hep-ex/0606006].
- 365 [10] M. Antonello *et al.*, “Muon momentum measurement in ICARUS-T600 LAr-TPC via multiple
366 scattering in few-GeV range,” arXiv:1612.07715 [physics.ins-det].
- 367 [11] G. R. Lynch and O. I. Dahl, Nucl. Instrum. Methods Section B (Beam Interactions with Materials
368 and Atoms) **B58**, **6** (1991).
- 369 [12] S. Agostinelli et al. Nucl. Instrum. Methods Phys. Res. **A506250-303** (2003)
- 370 [13] F. Cavanna *et al.* [LArIAT Collaboration], arXiv:1406.5560 [physics.ins-det].
- 371 [14] J. S. Marshall and M. A. Thomson, “The Pandora Software Development Kit for Pattern
372 Recognition,” Eur. Phys. J. C **75**, no. 9, 439 (2015) doi:10.1140/epjc/s10052-015-3659-3
373 [arXiv:1506.05348 [physics.data-an]].
- 374 [15] D. E. Groom, N. V. Mokhov and S. Striganov, “Muon Stopping Power and Range Tables: 10 MeV -
375 100 TeV” Table 5, <http://pdg.lbl.gov/2012/AtomicNuclearProperties/adndt.pdf>
- 376 [16] H. Bichsel, D. E. Groom, S.R. Klein, “Passage of Particles Through Matter” PDG Chapter 27, Figure
377 27.1 <http://pdg.lbl.gov/2005/reviews/passagerpp.pdf>
- 378 [17] Table 289: Muons in Liquid argon (Ar) http://pdg.lbl.gov/2012/AtomicNuclearProperties/MUON_ELOSS_TABLES/muonloss_289.pdf
- 380 [18] “Stopping Powers and Ranges for Protons and Alpha Particles,” ICRU Report No. 49 (1993); Tables
381 and graphs of these data are available at <http://physics.nist.gov/PhysRefData/>
- 382 [19] D. Heck, J. Knapp, J. N. Capdevielle, G. Schatz, T. Throw, *CORSIKA: A Monte Carlo Code to*
383 *Simulate Extensive Air Showers*, Forschungszentrum Karlsruhe Report FZKA 6019 (1998)